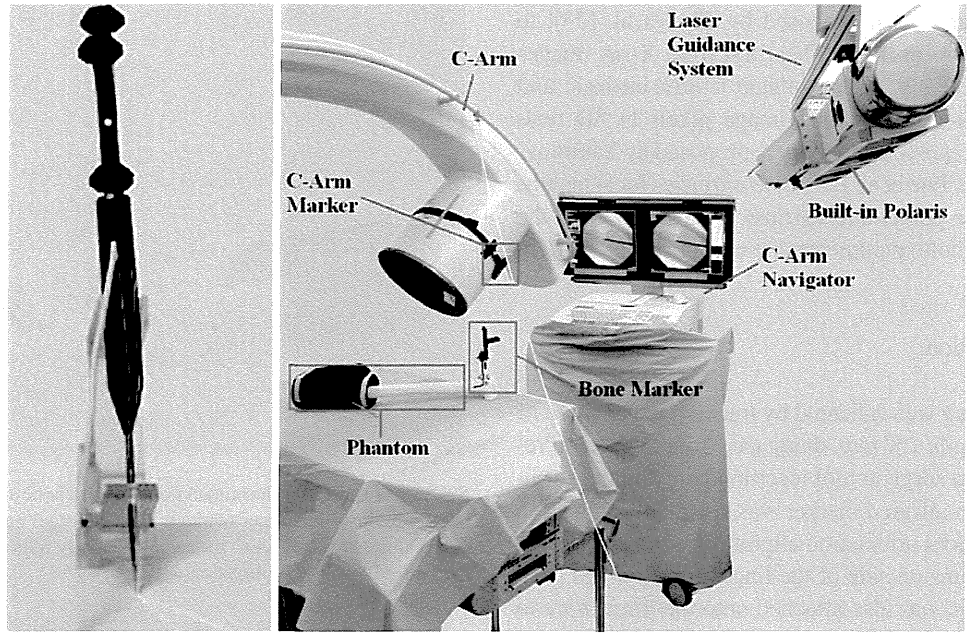

Fig. 3 *Left* proper orientation alignment is shown by parallel lasers on the side face of the linear wire with infrared marker and sleeve attached. *Right* experimental setup includes the laser guidance system with built-in optical tracking capabilities, a flat surface, a fluoroscopic C-arm, and a phantom. Infrared markers are used to locate the C-arm and phantom

point on the body surface or a target point inside the body. Using calibrated C-arm parameters described in the C-arm calibration section, this 2D plan is projected starting from the imaging device's pinhole and along its ray-lines to obtain a plane with normal vector n_i in 3D space. This plane is formulated in CS_F (Eq. 1) and transformed for use in CS_S (Eq. 2)

$$^{fluoro}T_{plane} = f_1\left(T_{calibration}, T_{plan2D}\right) \quad (1)$$

$$^{subject}T_{plane} = {T_{subject}}^{-1}\,T_{fluoro}\,^{fluoro}T_{plane} \quad (2)$$

Following Fig. 2, two 2D plans from two sets of inputs yield two planes, $plane_1$ and $plane_2$, in the 3D navigation space. The normal vectors of $plane_1$ and $plane_2$ are n_1 and n_2, respectively. The intersection of two planes yields a line in 3D space and is described by the point P_{int} and vector u_{int}. The directional vector, u_{int}, is the cross products of n_1 and n_2. The point P_{int} in 3D space is calculated by projecting points P_1 and P_2 into lines in 3D space and finding the point at which these projected lines traverse. This intersection line described by P_{int} and u_{int} represents the insertion path in 3D space.

If three sets of inputs are used, three 2D plans are made to give three planes in 3D space. This gives rise to three very similar intersection lines in 3D space with 3D points $\{P_{int1}, P_{int2}, P_{int3}\}$ and 3D directional vectors $\{u_{int1}, u_{int2}, u_{int3}\}$. Simple algebraic regression of these three lines is performed to obtain a line of best fit. A circle is fitted to P_{int1}, P_{int2}, and P_{int3}. We define P_{reg} as the center of this circle. Vector averaging of u_{int1}, u_{int2}, and u_{int3} yields u_{reg}. The regressed line represents the optimal tool insertion path (Eq. 3). This optimal insertion path is expressed by $^{subject}T_{plan3D}$ and stored in CS_S. Thus, it is robust toward any movements of the surgical object. The z-axis of the matrix corresponds to u_{reg}. Following Eq. (4), $^{subject}T_{plan3D}$ is transformed from CS_S into the localizer-laser coordinate systems. Next, this insertion path is projected by the laser sources. Finally, surgical navigation by laser guidance is achieved.

$$^{subject}T_{plan3D} = f_2\left(^{subject}T_{plane1}, {}^{subject}T_{plane2}, {}^{subject}T_{plane3}\right) \quad (3)$$

$$^{laser}T_{plan} = T_{laser}^{-1}\,T_{subject}\,^{subject}T_{plan3D} \quad (4)$$

C-arm calibration

Although the Siemens Arcadis Orbic C-arm is iso-centric and has 3D cone-beam reconstruction capabilities, we operated it under the Digital Radiography mode to better resemble an ordinary fluoroscopic X-ray. This system is serviced periodically and has a built-in geometric distortion correction function; consequently, additional distortion correction calibrations were not implemented. Accordingly, we assumed the C-arm to be a pinhole camera without distortion. A double-ring C-arm calibration phantom similar to that described by Livyatan et al. [22] but with 137 embedded fiducial steel ball bearings was used. We applied a cluster detection

algorithm, similar to that proposed by Cho et al. [23], to extract 2D positions of the ball bearings from X-ray images for calibration. Finally, we calculated C-arm intrinsic and extrinsic parameters by relating image pixels to 3D real-world points via equations previously proposed by Yakimovsky et al. [24] and Tate et al. [25]. The intrinsic (focal lengths and image-center point) and extrinsic (3D location of the image device pinhole) parameters are used for surgical planning.

Accuracy evaluation

Guidance accuracy was validated by tracking the position of a linear wire (length, 150 mm; diameter, 3 mm), which represented the desired surgical tool insertion path and the surgical tool itself. An infrared marker was attached for position tracking. Proper tool orientation alignment was indicated by parallel laser beams on side of the linear wire (Fig. 3) [15]. A guidance sleeve was also attached onto the linear wire to enlarge the wire's radius to better view projected laser lines.

We created a virtual coordinate system on a flat surface with its z-axis normal to the surface. We used a three factorial Box–Behnken (BB) experimental design method [26] to create 15 validation trials with different ground truth insertion path. These paths were each represented by a 4-by-4 transformation matrix. BB design factors and levels were as follows: xy-direction (−50/50, 0, 50/50 mm), polar angle (−30, 0, 30°), and azimuthal angle (−30, 0, 30°). Surgical planning was conducted using two 2D images taken at 90° angles for planning and three 2D images taken with 45° angle differences.

For each validation trial, the following procedure was performed. First, the ground truth insertion path was shown by the dual lasers in 3D space. The infrared attached linear wire was placed according to the lasers. Using this initial linear wire position, 2D images were taken for planning. The linear wire was removed while planning was performed. Once the 3D insertion path was generated, the laser was turned on. The linear wire was repositioned using guidance by laser. Final linear wire position was recorded once parallel laser beams were observed on the guidance sleeve. Proper alignment of linear wire with the laser beams required matching of five positional coordinates: the xyz translational coordinates, the polar angle (θ), and the azimuthal angle (ψ). The translational coordinates measured the laser's accurate Cartesian positioning of the insertion point. The two angles were used to determine alignment of the surgical tool during insertion, also referred to as insertion orientation.

Pin insertion using phantoms

The feasibility of the proposed system was tested by mimicking percutaneous guidewire insertion procedures common in fracture repair surgeries (Fig. 3). In this experiment, we inserted a total of 6 guidewire into 3 phantoms (Fig. 4) using commercially available orthopedic surgical tools from MicroAire. Bone structure and soft tissue were made of paint thinner coated plastic femur bone phantoms (SAWBONEs; SAWBONE Inc., USA) and polyvinyl chloride (Ludlow Composites, USA) of 30 mm thickness, respectively (Fig. 4). Realistically, bone and skin are not rigidly attached; thus, polyvinyl chloride was used to distort the actual location of the bone (Fig. 5). The patient coordinate system, CS_S, was created using an infrared marker attached to the sawbone.

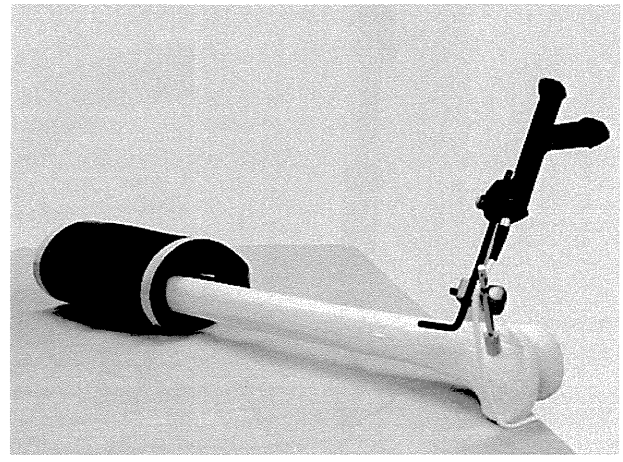

Fig. 4 A phantom of the human right femoral bone and soft tissue. Pedicle screw insertion experiments were performed on 3 phantoms. The material used to mimic soft tissue can be freely relocated depending on the desired location of insertion

Three X-ray images of the phantom were taken with angle difference of 45°. Insertions were separated into two categories: with anatomical landmark or with artificial landmark. In the former case, intramedullary nail insertion through the femoral head was performed. The shape of the femoral head acted as the anatomical landmark, and insertion plans were made through the center of the femoral head. In cases lacking anatomical landmarks, such as in bone reduction surgeries where insertions are made perpendicular to the bone shaft, artificial landmarks are provided. In our experiments requiring landmarks, a surgically used Kirschner (K) wire (MicroAire, Charlottesville, USA) placed perpendicular to the femur shaft of the phantom acted as the artificial landmark. The K-wire is linearly shaped, similar to the linear wire used for accuracy evaluation. We performed surgical planning referencing this K-wire. Upon completion, lasers were turned on and a guidewire was inserted. Each inserted guidewire was measured by locating its tip, the contact point with the phantom surface, and its end with an optically tracked stylus. Specifically, tip was calculated using three points on the guidewire circumference. Position and orientation errors were then given as the difference between each planned insertion and the final guidewire position in physical space.

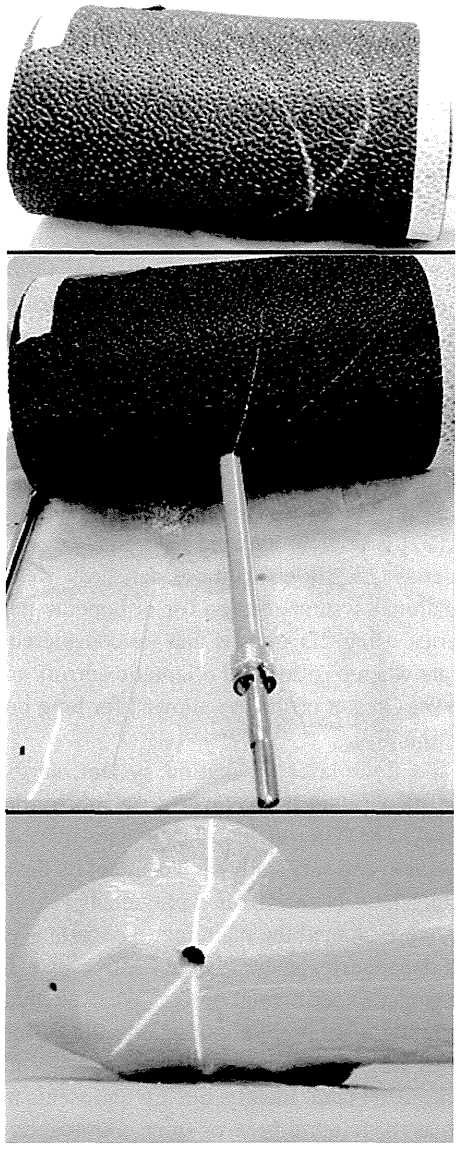

Fig. 5 *Top* laser being projected onto the phantom (femoral head cannot be visualized). *Middle* guidewire completely inserted into the phantom; proper orientation is indicated by parallel lasers. *Bottom* lasers being projected onto the bone after the removal of the soft tissue material and inserted guidewire

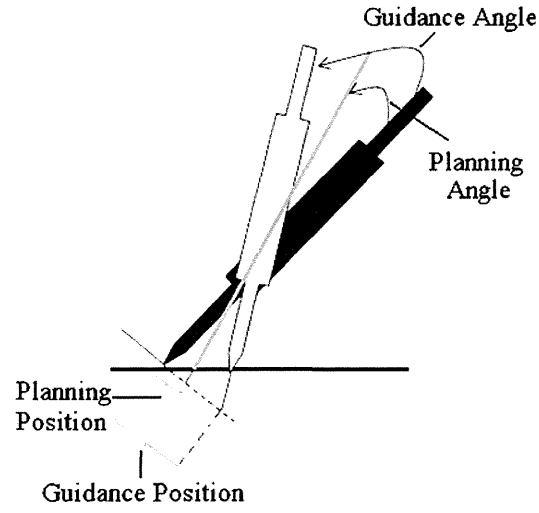

Fig. 6 The *black* needle represents the initial linear wire position; the *white* needle is the final linear wire position; and the *green* line is the planned insertion path in 3D space. Guidance error looks at the angular and positional differences between the initial and final needle positions. Planning error looks at the angular and positional differences between the initial needle position and planned insertion line

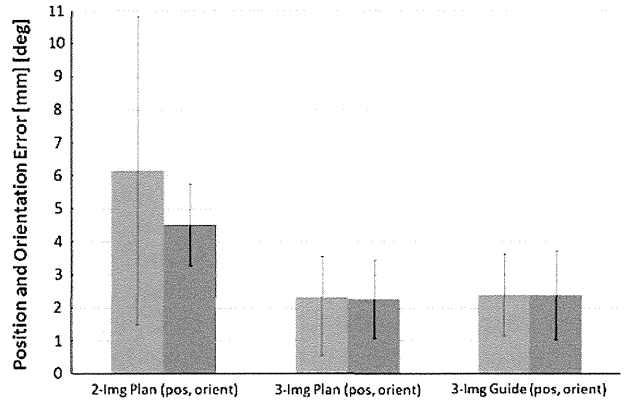

Fig. 7 Position and orientation errors shown in *blue* and *red*, respectively. Results include accuracies for 2-image planning, 3-image planning, and 3-image guidance

Results

Navigation accuracy

Fluorolaser accuracy validation looked at the displacement of relative tip locations between planed 3D insertion path, initial linear wire position, and final linear wire position. Since the binary lasers cannot indicate insertion depth, we report only the system's lateral errors. In particular, we calculated the difference in tip positions in a plane that is perpendicular and intersects the initial linear wire tip (Fig. 6). Planning accuracy refers to the error between actual insertion path and user-determined insertion path. A transformation matrix describing the user-generated 3D insertion path was obtained with its origin at the insertion point. Guidance accuracy refers to the error of the overall system. The two ends of the linear wire were registered to the attached AdapTrax marker. Thus, initial and final linear wire tip positions and orientation vectors in the world coordinate were obtained using simple transformation.

The results of the 15 validation trials are presented in Fig. 7. Planning accuracy of the system using two 2D images for planning was found to be 6.17 ± 4.68 mm, $4.53 \pm 1.24°$. Accuracy using linear regression of three 2D images for planning was found to be 2.32 ± 1.74 mm, $2.28 \pm 1.19°$. There

Table 1 Experimental results using physical space evaluation

	Femoral shaft insertion		Femoral head insertion	
Mean	2.05 (mm)	1.91°	2.12 (mm)	2.26°
SD	0.09 (mm)	0.70°	0.31 (mm)	2.26°
RMS	1.71 (mm)	1.73°	2.13 (mm)	2.26°

is a significant improvement in both position and orientation accuracy with the use of three images (P value: 1.06×10^{-2} and 1.21×10^{-4} for position and orientation, respectively).

Using three images, the RMS error of position and orientation accuracies was 2.86 mm and 2.55°, respectively. The overall guidance RMS error with the use of three 2D images was found to be 2.67 mm and 2.72° (2.40 ± 1.23 mm, 2.39 ± 1.34°). Moreover, Box–Behnken surface response analysis showed that no single factor in the 15 different three-factor three-level combinations (xy: − 50/50, 0, 50/50 mm; polar: −30, 0, 30°; azimuthal: −30, 0, 30°) contributed significantly more to the planning and guidance errors.

Phantom feasibility

We performed percutaneous guidewire insertion experiments using 3 sawbone phantoms for a total of 6 insertions: 3 perpendicular to the femur shaft and 3 through the femoral head. We performed feasibility analysis visually as well as by comparing the planning matrix and the final inserted guidewire position. A summary of the lateral errors is shown in Table 1. We obtained an RMS error of 1.71 mm and 1.73° for femoral shaft insertions using artificial landmark. Femoral head insertion using anatomical landmark (Fig. 8) yielded RMS error of 2.13 mm and 2.26°. Differences between femoral head and shaft insertions were not significant. Max error between all 6 insertions was 2.35 mm, 2.63°.

Visually, we observed parallel laser lines on the referenced K-wire in trials where artificial landmarks were used. The average overall operation time from image acquisition to insertion completion per insertion was less than 10 min. Average time for planning was 1 min and 8 s, where planning using anatomical landmarks took on average 1 min and 25 s and trials with artificial landmarks took 51 s. Drilling and insertion of the guidewire was the most time-consuming step in the entire operation.

Discussion

The Gertzbein and Robbins pedicular screw placement classification [27] is commonly used to evaluate accuracies of spine surgeries [28,29]. Using these standards, we conclude that navigational systems design for orthopedic percutaneous surgeries using 2D images can be considered precise and accurate when position and orientation errors are within 2 mm and 2°. Greater errors are allowed for long bone fracture reduction [30].

Using the fluorolaser navigation system, surgical outcomes can be affected by navigation accuracy and execution accuracy. The latter includes accuracies related to laser beam projection and surgical tool placement by the surgeon, both of which have been validated previously [15,20,21]. In this study, we evaluated the planning (navigation) error and overall guidance error of the system using a Box–Behnken surface response experimental design. We evaluated the lateral positioning error by computing the 2D difference of tip positions in a plane that is perpendicular to and intersects the insertion plan. Ideally, this tip represents the target point such as the femoral bone or spine. Our results indicate

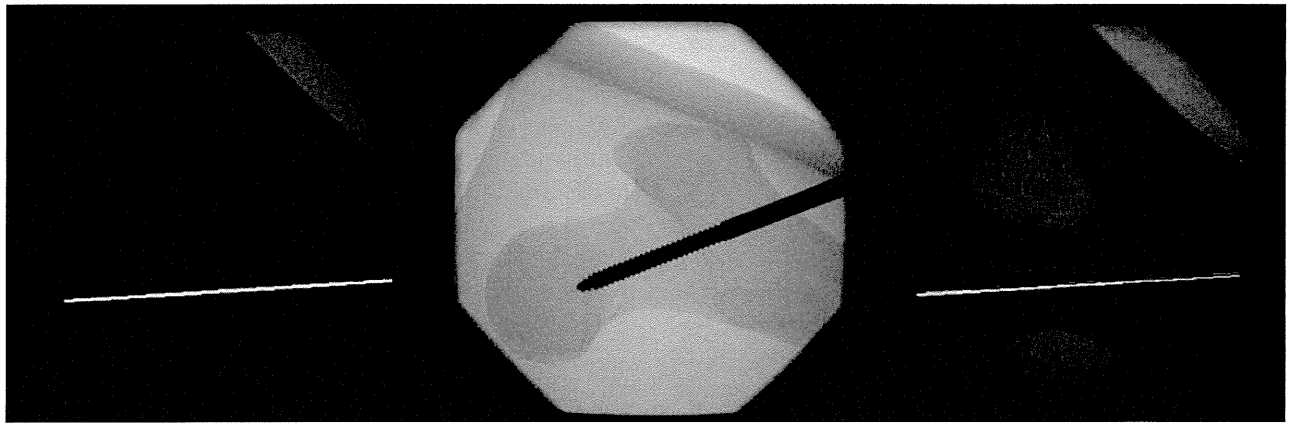

Fig. 8 X-ray images of a phantom containing the femoral head and soft tissue. *Left* X-ray image with insertion plan line shown in green. *Center* X-ray image of the phantom after pin insertion. *Right* overlay of insertion plan onto the center image

that while the accuracies are acceptable, the current system is not yet robust enough for clinical usage due to the high standard deviation. Furthermore, planning accuracy is limited by the C-arm fluoroscope calibration technique as well as user-based insertion path planning procedure. In the current calibration protocol, 100 fiducial marker positions in 2D and 3D were obtained via image processing and calculations, respectively. Compared with the laser guidance system using CT-based navigation, which had a phantom guidewire insertion RMS error of 1.39 mm, 1.03° [15], future calibration protocol should consider the increase in fiducial count or the use of multiple phantom images taken from different positions to improve system accuracy. Also, the current study took X-ray C-arm images only in one C-arm rotational plane. Future studies should consider the effects of relative C-arm positions toward accuracy.

The current planning procedure requires the aid of structural landmarks present on the X-ray image. This is the key to simplifying the interpretation of 3D positions from 2D images. However, anatomical landmarks may not always be available for all types of surgeries. Although no significant differences are detected between insertions made with and without anatomical landmarks, additions should be made onto the current system to ensure a simple and efficacious planning procedure. We intend to introduce artificial landmarks in the form of radiopaque stickers to be attached onto the patient skin. Nevertheless, the planning interface can be modified accordingly depending on the specific surgical task required.

We performed phantom experiments to validate the capabilities of percutaneous pin insertion procedures. Intraoperatively guidance was intuitive and insertion procedures were not interfered by the surrounding environment. Although fracture reduction surgery was one of the targeted surgical procedures of the original laser guidance system, we were unable to perform reduction experiments using the improved fluorolaser system. This was because relative insertion positions are essential in fixation-based reduction [31]. Future works should investigate other methods, such as visual servoing [32], to apply this new system into reduction surgeries. Furthermore, this study focused on orthopedic percutaneous surgeries; however, use of the dyna-CT function in X-ray C-arms may allow the proposed system to be useful in surgeries involving linear insertions into soft tissues.

Another future requirement is the introduction of insertion depth guidance. Depth guidance may be achieved using additional X-rays or attaching positioning trackers onto the tool. The former method would increase radiation exposure, while the latter introduces specialized surgical tools that limit the range of motion of surgeons during interventions. Another approach is to introduce additional mechanisms such as a physical stopper, a physical depth guide, or a depth guidance ring onto the surgical tool and surgical drill. Some surgical procedures currently use these types of tools. Also, a third laser source may also be a viable method that can guide depth without additional visualization mechanisms. Without additional mechanisms, this fluorolaser navigation system can only be used for surgical procedures that use surgical drills with depth guidance rings on their shaft. Nevertheless, addition of depth guidance may widely expand the applicable areas of our method.

Moving away from the conventional surgical navigation systems, we have presented the fluorolaser system, which allows navigated surgeries to be performed simply by aligning surgical tools at the crosshair of two laser beams. Surgical planning is performed using three X-ray images as opposed to complete CT. The system does not require surgeons to obtain navigation information from a secondary display source. This system does not require specialized or tracked surgical tools; it can thus be easily integrated into many surgical environments. Although this system is an improvement to conventional systems, future improvements and clinical assessments are necessary to fully validate its robustness in actual surgeries.

Conclusion

In conclusion, we have proposed the fluorolaser navigation system, which combines the fluoroscope-based navigation and laser guidance techniques to enable intuitive positioning of linear surgical tools to be inserted in percutaneous surgeries without preoperative CT/MRI volumes. Specifically, in vitro needle insertion path planning and phantom pedicle screw insertion experiments were performed using three 2D X-ray images from a C-arm and two laser beams for insertion guidance. Since the binary lasers cannot indicate insertion depth, we report only the system's lateral errors. Experimental results demonstrate that the fluorolaser navigation system has great potentials to ensure accurate and intuitive surgical tool insertion procedures without preoperative CT/MRI volumes and registration processes.

Conflict of interest None.

References

1. Schlenzka D, Laine T, Lund T (2000) Computer-assisted spine surgery. Eur Spine J 9(7):57–64. doi:10.1007/PL00010023
2. Fuchs H, State A, Pisano E, Garrett W, Hirota G, Livingston M, Whitton M, Pizer S (1996) Towards performing ultrasound-guided needle biopsies from within a head-mounted display visualization in biomedical computing. In: Höhne K, Kikinis R (eds), vol 1131. Lecture notes in computer science. Springer, Berlin, Heidelberg, pp 591–600. doi:10.1007/BFb0047002
3. Blackwell M, Nikou C, DiGioia AM, Kanade T (2000) An image overlay system for medical data visualization. Med Image Anal 4(1): 67–72. doi:10.1016/s1361-8415(00)00007-4

4. Fichtinger G, Deguet A, Masamune K, Balogh E, Fischer GS, Mathieu H, Taylor RH, Zinreich SJ, Fayad LM (2005) Image overlay guidance for needle insertion in CT scanner. IEEE Trans Biomed Eng 52(8):1415–1424
5. Liao H, Ishihara H, Tran H, Masamune K, Sakuma I, Dohi T (2008) Fusion of laser guidance and 3-D autostereoscopic image overlay for precision-guided surgery medical imaging and augmented reality. In: Dohi T, Sakuma I, Liao H (eds), vol 5128. Lecture notes in computer science. Springer, Berlin, Heidelberg, pp 367–376. doi:10.1007/978-3-540-79982-5_40
6. Volonté F, Pugin F, Bucher P, Sugimoto M, Ratib O, Morel P (2011) Augmented reality and image overlay navigation with OsiriX in laparoscopic and robotic surgery: not only a matter of fashion. J Hepato-Biliary-Pancreatic Sci 18(4): 506–509. doi:10.1007/s00534-011-0385-6
7. Gavaghan K, Oliveira-Santos T, Peterhans M, Reyes M, Kim H, Anderegg S, Weber S (2011) Evaluation of a portable image overlay projector for the visualisation of surgical navigation data: phantom studies. Int J Comput Assist Radiol Surg. doi:10.1007/s11548-011-0660-7
8. Malik JM, Kamiryo T, Goble J, Kassell NF (1995) Stereotactic laser-guided approach to distal middle cerebral artery aneurysms. Acta Neurochirurgica 132(1):138–144. doi:10.1007/bf01404862
9. Lavallee S, Toroccaz J, Sautot P et al (1996) Computer-assisted spinal surgery using anatomy-based registration. In: Computer-Integrated Surgery: Technology and Clinical Applications, the MIT Press, pp 425–229
10. Hussman KL, Chalouplca JC, Berger SB (1998) Frameless laser-guided stereotaxis: a system for CT-monitored neurosurgical interventions. Stereotect Funct Neurosurg 71:62–75. doi:10.1159/000029649
11. Glossop N, Wedlake C, Moore J, Peters T, Wang Z (2003) Laser projection augmented reality system for computer assisted surgery medical image computing and computer-assisted intervention—MICCAI 2003. In: Ellis R, Peters T (eds), vol 2879. Lecture Notes in Computer Science. Springer, Berlin, Heidelberg, pp 239–246. doi:10.1007/978-3-540-39903-2_30
12. Marmurek J, Wedlake C, Pardasani U et al (2005) Image-guided laser projection for port placement in minimally invasive surgery. In: Medicine meets virtual reality 14, vol 119. IOS Press, pp 367–372
13. Nitta N, Takahashi M, Tanaka T, Takazakura R, Sakashita Y, Furukawa A, Murata K, Shimoyama K (2007) Laser-guided computed tomography puncture system: simulation experiments using artificial phantom lesions and preliminary clinical experience. Radiat Med 25(4):187–193. doi:10.1007/s11604-006-0116-0
14. Sasama T, Sugano N, Sato Y, Momoi Y, Koyama T, Nakajima Y, Sakuma I, Fujie M, Yonenobu K, Ochi T, Tamura S (2002) A novel laser guidance system for alignment of linear surgical tools: its principles and performance evaluation as a man—machine system medical image computing and computer-assisted intervention—MICCAI 2002. In: Dohi T, Kikinis R (eds) vol 2489. Lecture notes in computer science. Springer, Berlin, Heidelberg, pp 125–132. doi:10.1007/3-540-45787-9_16
15. Nakajima Y, Sasama T, Momoi Y, Sugano N, Tamura Y, Dohi T, Lim S, Sakuma I, Mitsuishi M, Koyama T, Yonenobu K, Ohnishi I, Bessho M, Ohashi S, Nakamura K (2012) Surgical tool alignment guidance by drawing two cross-sectional laser-beam planes. IEEE Trans Biomed Eng (in-press)
16. Foley KT, Simon DA, Rampersaud YR (2001) Virtual fluoroscopy: computer-assisted fluoroscopic navigation. Spine 26(4):347–351
17. Hofstetter R, Slomczykowski M, Sati M, Nolte L-P (1999) Fluoroscopy as an imaging means for computer-assisted surgical navigation. Comput Aided Surg 4(2): 65–76. doi:10.3109/10929089909148161
18. Wiest P, Locken J, Heintz P, Mettler F (2002) CT scanning: a major source of radiation exposure. Semin Ultsd CT MRI 23(5):402–410. doi:10.1053/sult.2002.34010
19. Smith H, Welsch M, Sasso R, Vaccaro A (2008) Comparison of radiation exposure in lumbar pedicle screw placement with fluoroscopy vs computer-assisted image guidance with intraoperative three-dimensional imaging. J Spinal Cord Med 31(5):532–537
20. Nakajima Y, Yamamoto H, Sato Y, Sugano N, Momoi Y, Sasama T, Koyama T, Tamura Y, Yonenobu K, Sakuma I, Yoshikawa H, Ochi T, Tamura S (2004) Available range analysis of laser guidance system and its application to monolithic integration with optical tracker. Int Congr Ser 1268(0): 449–454. doi:10.1016/j.ics.2004.03.127
21. Lim S, Douke T, Onogi S et al (2010) Assessment for the feasibility of external-fixation pin guidance using laser navigation. Jpn Soc Comp Aid Surg 12:511–518
22. Livyatan H, Yaniv Z, Joskowicz L (2002) Robust automatic C-arm calibration for fluoroscopy-based navigation: a practical approach medical image computing and computer-assisted intervention—MICCAI 2002. In: Dohi T, Kikinis R (eds) vol 2489. Lecture notes in computer science. Springer, Berlin, Heidelberg, pp 60–68. doi:10.1007/3-540-45787-9_8
23. Cho PS, Johnson RH (1998) Automated detection of bb pixel clusters in digital fluoroscopy images. Phys Med Biol 42:2677–2682
24. Yakimovsky Y, Cunningham R (1978) A system for extracting three-dimensional measurements from a stereo pair of TV cameras. Comput Graph Image Process 7(2):195–210. doi:10.1016/0146-664x(78)90112-0
25. Tate P, Lachine V, Fu L, Croitoru H, Sati M (2001) Performance and robustness of automatic fluoroscopic image calibration in a new computer assisted surgery system medical image computing and computer-assisted intervention—MICCAI 2001. In: Niessen W, Viergever M (eds) vol 2208. Lecture notes in computer science. Springer, Berlin, Heidelberg, pp 1130–1136. doi:10.1007/3-540-45468-3_135
26. Ferreira S, Bruns R, Ferreira H, Matos G, David J, Brandao G, Silva E, Portugal L, Reis P, Souza A, Santos W (2007) Box-Behnken design: an alternative for the optimization of analytical methods. Analytica Chimica Acta 597(2):179–186. doi:10.1016/j.aca.2007.07.011
27. Gertzbein S, Robbins S (1990) Accuracy of pedicular screw placement in vivo. Spine 15(1):11–14
28. Pechlivanis I, Kiriyanthan G, Engelhardt M, Scholz M, Lucke S, Harders A, Schmieder K (2009) Percutaneous placement of pedicle screws in the lumbar spine using a bone mounted miniature robotic system. Spine 34(4):392–398
29. Belmont P, Klemme W, Dhawan A, Polly D (2001) In vivo accuracy of thoracic pedicle screws. Spine 26(21):2340–2346
30. Weil Y, Liebergall M, Mosheiff R, Helfet D, Pearle A (2007) Long bone fracture reduction using a fluoroscopy-based navigation system: a feasibility and accuracy study. Comp Aided Surg 12(5): 295–302
31. Navab N, Bascle B, Loser M, Geiger B, Taylor R (2000) Visual servoing for automatic and uncalibrated needle placement for percutaneous procedures. In: Proceedings of the IEEE Conference on Computer vision and pattern recognition, 2000, vol.322. pp 327–334
32. Croitoru H, Ellis RE, Prihar R, Small CF, Pichora DR (2001) Fixation-based surgery: a new technique for distal radius osteotomy. Comput Aided Surg 6(3):160–169. doi:10.1002/igs.1019

Cancer Chemother Pharmacol (2013) 71:511–521
DOI 10.1007/s00280-012-2041-5

ORIGINAL ARTICLE

Randomized trial of chemoradiotherapy and adjuvant chemotherapy with nimustine (ACNU) versus nimustine plus procarbazine for newly diagnosed anaplastic astrocytoma and glioblastoma (JCOG0305)

Soichiro Shibui · Yoshitaka Narita · Junki Mizusawa · Takaaki Beppu · Kuniaki Ogasawara · Yutaka Sawamura · Hiroyuki Kobayashi · Ryo Nishikawa · Kazuhiko Mishima · Yoshihiro Muragaki · Takashi Maruyama · Junichi Kuratsu · Hideo Nakamura · Masato Kochi · Yoshio Minamida · Toshiaki Yamaki · Toshihiro Kumabe · Teiji Tominaga · Takamasa Kayama · Kaori Sakurada · Motoo Nagane · Keiichi Kobayashi · Hirohiko Nakamura · Tamio Ito · Takahito Yazaki · Hikaru Sasaki · Katsuyuki Tanaka · Hideaki Takahashi · Akio Asai · Tomoki Todo · Toshihiko Wakabayashi · Jun Takahashi · Shingo Takano · Takamitsu Fujimaki · Minako Sumi · Yasuji Miyakita · Yoichi Nakazato · Akihiro Sato · Haruhiko Fukuda · Kazuhiro Nomura

Received: 6 October 2012 / Accepted: 22 November 2012 / Published online: 11 December 2012

Abstract
Purpose Glioblastoma (GBM) is one of the worst cancers in terms of prognosis. Standard therapy consists of resection with concomitant chemoradiotherapy. Resistance to nimustine hydrochloride (ACNU), an alkylating agent, has been linked to methylguanine DNA methyltransferase (MGMT). Daily administration of procarbazine (PCZ) has been reported to decrease MGMT activity. This study investigated the efficacy of ACNU + PCZ compared to ACNU alone for GBM and anaplastic astrocytoma (AA).

Methods Patients (20–69 years) who had newly diagnosed AA and GBM were randomly assigned to receive radiotherapy with ACNU alone or with ACNU + PCZ. The primary endpoint was overall survival (OS). This was designed as a phase II/III trial with a total sample size of 310 patients and was registered as UMIN-CTR C000000108.
Results After 111 patients from 19 centers in Japan were enrolled, this study was terminated early because temozolomide was newly approved in Japan. The median OS and median progression-free survival (PFS) with ACNU alone ($n = 55$) or ACNU + PCZ ($n = 56$) in the

S. Shibui (✉) · Y. Narita · Y. Miyakita · K. Nomura
Department of Neurosurgery and Neuro-Oncology,
National Cancer Center Hospital, 5-1-1,
Tsukiji, Chuo-ku, Tokyo 104-0045, Japan
e-mail: sshibui@ncc.go.jp

J. Mizusawa · A. Sato · H. Fukuda
Japan Clinical Oncology Group Data Center,
National Cancer Center, Tokyo, Japan

T. Beppu · K. Ogasawara
Department of Neurosurgery, Iwate Medical University,
Iwate, Japan

Y. Sawamura · H. Kobayashi
Department of Neurosurgery, Hokkaido University Graduate
School of Medicine, Hokkaido, Japan

R. Nishikawa · K. Mishima
Department of Neuro-Oncology/Neurosurgery,
International Medical Center, Saitama Medical University,
Saitama, Japan

Y. Muragaki · T. Maruyama
Department of Neurosurgery,
Tokyo Women's Medical University, Tokyo, Japan

J. Kuratsu · H. Nakamura · M. Kochi
Department of Neurosurgery,
Kumamoto University,
Kumamoto, Japan

Y. Minamida · T. Yamaki
Department of Neurosurgery,
Sapporo Medical University,
Sapporo, Japan

T. Kumabe · T. Tominaga
Department of Neurosurgery,
Tohoku University School of Medicine, Miyagi, Japan

T. Kayama · K. Sakurada
Department of Neurosurgery, Faculty of Medicine,
Yamagata University, Yamagata, Japan

intention-to-treat population were 27.4 and 22.4 months ($p = 0.75$), and 8.6 and 6.9 months, respectively. The median OS and median PFS of the GBM subgroup treated with ACNU alone ($n = 40$) or ACNU + PCZ ($n = 41$) were 19.0 and 19.5 months, and 6.2 and 6.3 months, respectively. Grade 3/4 hematologic adverse events occurred in more than 40 % of patients in both arms, and 27 % of patients discontinued treatment because of adverse events.

Conclusions The addition of PCZ to ACNU was not beneficial, in comparison with ACNU alone, for patients with newly diagnosed AA and GBM.

Keywords Glioblastoma · Anaplastic astrocytoma · Nimustine · ACNU · Procarbazine · MGMT

Abbreviations

GBM	Glioblastoma
AA	Anaplastic astrocytoma
ACNU	Nimustine hydrochloride
BCNU	Carmustine
TMZ	Temozolomide
MGMT	Methylguanine DNA methyltransferase
WHO	World Health Organization
PFS	Progression-free survival
OS	Overall survival
RT	Radiotherapy
HR	Hazard ratio
AE	Adverse event
ND	Not determined
CR	Complete response
PR	Partial response
SD	Stable disease
PD	Progressive disease
WBC	White blood cell
3D-CRT	Three-dimensional conformal radiotherapy
CT	Computed tomography
IMRT	Intensity-modulated radiation therapy
BEV	Beam's eye views
DVH	Dose–volume histograms
GTV	Gross tumor volume
CTV	Clinical target volume
PTV	Planning target volume
ICRU	International Commission on Radiation Units
FLAIR	Fluid-attenuated inversion recovery
OAR	Organ-at-risk

Introduction

Glioblastoma (GBM) is one of the worst cancers in terms of prognosis, with almost all patients experiencing progression without cure. According to the report of the Brain Tumor Registry of Japan, the %5-year survival of World Health Organization (WHO) grade IV GBM is 6.9 % and that of WHO grade III anaplastic astrocytoma (AA) is 33.9 % [1].

Standard therapy against GBM consists of the maximal resection that is safely possible, with concomitant chemo-radiotherapy. Currently, temozolomide (TMZ) is the

M. Nagane · K. Kobayashi
Department of Neurosurgery,
Kyorin University Faculty of Medicine, Tokyo, Japan

H. Nakamura · T. Ito
Department of Neurosurgery,
Nakamura Memorial Hospital, Hokkaido, Japan

T. Yazaki · H. Sasaki
Department of Neurosurgery,
Keio University School of Medicine, Tokyo, Japan

K. Tanaka
Department of Neurosurgery, St. Marianna University
School of Medicine, Kanagawa, Japan

H. Takahashi
Department of Neurosurgery, Brain Research Institute,
Niigata University, Niigata, Japan

A. Asai
Department of Neurosurgery,
Saitama Medical Center, Saitama, Japan

T. Todo
Department of Neurosurgery, University of Tokyo, Tokyo, Japan

T. Wakabayashi
Department of Neurosurgery, Nagoya University Graduate
School of Medicine, Nagoya, Japan

J. Takahashi
Department of Neurosurgery,
Kyoto University Graduate School of Medicine,
Kyoto, Japan

S. Takano
Department of Neurosurgery, Tsukuba University,
Tsukuba, Japan

T. Fujimaki
Department of Neurosurgery,
Teikyo University School
of Medicine, Tokyo, Japan

M. Sumi
Department of Radiation-Oncology,
National Cancer Center Hospital,
Tokyo, Japan

Y. Nakazato
Department of Pathology,
Gunma University, Gunma, Japan

standard agent used in the treatment of GBM. However, before the TMZ era, nitrosourea had been widely used for GBM and AA. The Glioma Meta-analysis Trialists Group described that chemotherapy including nitrosourea showed significant prolongation of survival, with a hazard ratio of 0.85 ($p < 0.0001$) [2].

Nimustine hydrochloride (ACNU) was developed in Japan, and for more than 20 years since 1980, it has been the standard chemotherapeutic agent against gliomas [3]. Wolff et al. [4] analyzed 364 studies, including a total of 24,193 patients with high-grade glioma, and reported that the survival gain in the 15 ACNU-treated cohorts was 8.9 months, compared to those who received different drugs or no chemotherapy. Takakura et al. [5] reported that the overall survival (OS) of AA and GBM treated by radiotherapy (RT) and concomitant ACNU were 36 and 12 months, respectively. Furthermore, the response rate of a more than 50 % reduction in tumor size was 46.2 % in both AA and GBM. Alkylating agents, including ACNU and procarbazine (PCZ), confer cytotoxic effects on glioma cells by alkylation at the O^6-position of guanine in DNA. This results in the formation of DNA cross-links [6]. Methylguanine DNA methyltransferase (MGMT) removes methylation damage induced by nitrosourea from the O^6-position of DNA guanines before cell injury, and this enzyme was detectable in 76 % of glioma tissues [7]. MGMT in glioma cells is a primary defense against nitrosourea, but the cellular methyltransferase activity of MGMT is exhausted after MGMT takes effect. Daily administration of PCZ for 10 days was reported to cause the accumulation of O^6-methylguanine; it also decreased MGMT activity in rat liver [8] and lymphocytes in lymphoma patients [9]. Inhibition of MGMT by O^6-benzylguanine increased the cytotoxicity of TMZ and carmustine (BCNU) to tumor cells [10]. From these results, it can be predicted that daily administration of PCZ, by depleting MGMT activity, will increase the efficacy of ACNU against AA and GBM.

To prove this hypothesis and establish a more potent standard therapy for AA and GBM, the Brain Tumor Study Group of the Japan Clinical Oncology Group (JCOG) conducted this clinical trial. The study was terminated at the end of the phase II part. The current report describes the final outcome of the study.

Subjects and methods

Patient eligibility criteria

Patients aged 20 to less than 70 years of age who had newly diagnosed and histologically proven supratentorial GBM or AA were eligible for this study. Patients were enrolled between 3 and 14 days after their operation. To be eligible, a patient's preoperative MRI had to show that more than 50 % of the tumor was located in supratentorial areas, except the optic nerve, olfactory nerve, or pituitary gland. Eligible patients had Eastern Cooperative Oncology Group (ECOG) performance status (PS) of 0–2 or 3 (only in cases with neurologic symptoms caused by a tumor) and adequate hematologic, pulmonary, renal, and hepatic function, defined as follows: white blood cell (WBC) count $\geq 3.0 \times 10^3$/mL, hemoglobin level ≥ 8.0 g/dL, platelets count $\geq 1.0 \times 10^6$/mL, aspartate transaminase (AST) level ≤ 100 IU/L, alanine transaminase (ALT) level ≤ 100 IU/L, serum creatinine level ≤ 1.0 mg/dL. Additionally, written informed consent was obtained from all the participating patients. We excluded patients with multiple or disseminated tumors or large tumors in which the planned target volume for irradiation exceeded 1/3 of the whole-brain volume. Additionally, we also classified as ineligible any patient who was pregnant, had meningitis, pneumonia, diabetes mellitus with insulin injection, myocardial infarction, or unstable angina pectoris within the last 3 months, mental disorders, a history of pulmonary fibrosis or interstitial pneumonia, or other forms of active cancer occurring within 5 years of treatment. The study protocol was approved by JCOG Protocol Review Committee and institutional review board at each center.

Treatment

After the confirmation of the eligibility criteria, registration was made by telephone or fax to the JCOG Data Center. Patients were randomized within 14 days of surgery to either ACNU with RT (the control arm, A) or to ACNU + PCZ with RT (the experimental arm, B) (Fig. 1a) by a minimization method with adjustment factors consisting of histology (GBM vs. AA), age (younger than 60 vs. 60 years or older), residual tumor (presence vs. absence), and institution. Residual tumor was assessed using a gadolinium-enhanced MRI obtained within 72 h of the surgery.

Radiotherapy with concomitant chemotherapy was started within 3 weeks after the surgery. Patient positioning and immobilization with an individual head mask and computed tomography (CT)-based planning were required. Treatment was delivered using linear accelerators with nominal energies ≥ 4 MV. Intensity-modulated radiation therapy (IMRT) technique was not permitted. All fields were to be treated every day. Three-dimensional conformal radiotherapy (3D-CRT) planning including the use of beam's eye views (BEV) and dose–volume histograms (DVH) were recommended for volumetric dose evaluation. Quality assurance reviews were done at the Radiotherapy Support Centre in Tokyo, Japan, with feedback sent to each

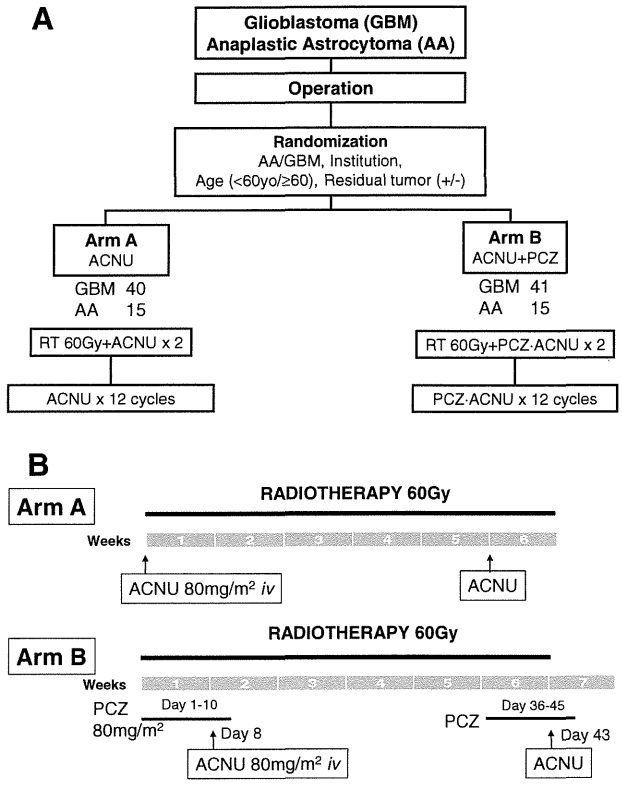

Fig. 1 **a** Study design of JCOG 0305: RT + ACNU versus RT + ACNU + PCZ; 40 patients with GBM and 15 patients with AA were assigned to *arm A*, and 41 patients with GBM and 15 patients with AA were assigned to *arm B*. **b** Treatment schedule of RT + ACNU (*Arm A*) and RT + ACNU + PCZ (*Arm B*)

institution by the radiotherapy study coordinator (Minako Sumi). The minimum and maximum dose to the PTV should be comprised between 95 and 107 % of the International Commission on Radiation Units (ICRU) reference point dose. The gross tumor volume (GTV) was defined as the primary tumor with or without enhancement on CT or magnetic resonance imaging (MRI). The clinical target volume 1(CTV1) included GTV, the resection cavity and surrounding edema (high-intensity area on T2-weighted or fluid-attenuated inversion recovery (FLAIR) image) plus a 1.5-cm margin. The CTV2 included GTV and the resection cavity plus a 1.5-cm margin. Planning target volume (PTV) was defined as CTV plus a margin of 0.5 cm or more. The doses for PTV1 and PTV2 were 50 and 10 Gy, respectively. The protocol required contouring organ-at-risk (OAR), including optic chiasm, brain stem, and retina. Cumulative doses to the optic chiasm and brainstem were limited to a maximum dose of 50 and 45 Gy for the retina.

In the control arm A, 80 mg/m^2 of ACNU was administered intravenously on days 1 and 36 during RT (Fig. 1b). In the experimental arm B, 80 mg/m^2 of oral PCZ was administered daily from days 1 to 10 and days 36 to 45, and given together with intravenous ACNU (80 mg/m^2) on days 8 and 43. Adjuvant therapy consisting of 80 mg/m^2 of ACNU alone in arm A or ACNU plus PCZ (PCZ: 80 mg/m^2 orally on days 1–10, ACNU: 80 mg/m^2 intravenously on day 8) in arm B started 56 days from the final administration of ACNU and was given every 8 weeks, for up to 12 cycles. Doses of ACNU and PCZ were calculated using actual body surface area, reduced for toxicity, and were not escalated.

Evaluations and follow-up

Baseline and follow-up examinations included vital signs, subjective symptoms, neurologic examination, MRI scan, and blood and serum laboratory examinations. For each patient, these examinations were performed weekly, with the exception of MRI scans, which were performed between the end of the initial chemoradiotherapy and the beginning of adjuvant therapy. All examinations were performed before each cycle of adjuvant chemotherapy, at a frequency of nearly every 2 months. After completion of the treatment protocol, patients were assessed every 3 months until progression. Toxicity was graded using the National Cancer Institute Common Toxicity Criteria (version 2). Findings of radiation necrosis were also assessed on MRI. Each patient was required to undergo a follow-up examination for at least 2 years from the date of randomization.

Tumor progression on MRI was defined according to Response Evaluation Criteria in Solid Tumors (RECIST), version 1.0 [11]. Progression of disease was defined as a 20 % increase in tumor size, as shown by contrast-enhanced imaging, or the development of new lesions, neurologic deterioration, or death by any cause. Further treatment at recurrence or progression was discretionary, but recorded.

A central pathology review by 3 independent pathologists (Yoichi Nakazato, a member of the Working Group for WHO 2007 classification; Nobuaki Funata; and Toru Iwaki) was performed and determinations given. A central review of radiological response was also performed.

Statistical analysis

When we planned this study, TMZ had been widely approved and was used worldwide. However, TMZ was not available in Japan. ACNU remained the standard therapy in Japan, but there was no sufficient data regarding this treatment. We planned a phase II/III clinical trial, with the phase II part designed to confirm the feasibility of ACNU and ACNU + PCZ.

The primary and secondary endpoints for the phase II part were %6-month survival and adverse events (AEs) in ACNU + PCZ arm. The primary endpoint of the phase III part was OS, while the secondary endpoints were PFS, response rate, complete response rate, and AEs.

Overall survival was calculated from the date of random assignment to the date of death from any cause and censored at the last follow-up for event-free patients. PFS was calculated from the date of randomization to the date of progression or death from any cause and censored at the last verifiable progression-free date for event-free patients. OS and PFS were estimated by the Kaplan–Meier method. OS was analyzed by the stratified log-rank test for eligible patients with adjustment factors, excluding institution. Unstratified log-rank tests were used for the analysis of PFS and subgroup analyses of OS and PFS. Fisher's exact test was used for categorical data. All p values are two-sided, except for primary analysis of OS.

We assumed %2-year survivals in AA and GBM for arm A were 50 and 20 %, and the ratio of those patients with AA or GBM enrolled in this study was expected to be 2:3. The phase III study was designed to enroll 155 patients per arm with 5 years of accrual and 2 years of follow-up, including those for the phase II part and about 10 % of ineligible patients, to achieve at least 75 % power to detect a hazard ratio (HR) of 0.74, with a one-sided alpha of 0.05 [12].

Three interim analyses were planned. The first was planned during phase II to test whether %6-month survival in arm A was superior to the predefined threshold (80 %), with a one-sided alpha of 0.1 and beta of 0.2, when 56 patients were included in ACNU + PCZ arm. The second and third interim analyses of OS were planned during phase III. For analyses of phase III part, multiplicity was adjusted by the Lan and DeMets alpha-spending function with the O'Brien and Fleming stopping boundary to control the type I error for primary endpoint.

In March 2007, protocol was amended to stop patient accrual after 111 patients had enrolled and to carry out the final analysis without planned interim analyses for both of phase II and phase III part. This was done because toxicity of both arms was unexpectedly high in phase II and because TMZ became available in Japan.

All statistical analyses were performed using SAS software, release 9.1 (SAS Institute, Cary, NC).

This trial is registered with UMIN-CTR (www.umin.ac.jp/ctr/), number C000000108.

Results

Patient characteristics

A total of 111 patients from 19 centers were randomly assigned to arm A ($n = 55$) or arm B ($n = 56$) from March 2004 to September 2006. Primary analyses were performed in September 2007, and the updated analyses were completed in July 2009. All patients were eligible for this study. Baseline characteristics were well balanced between the arms (Table 1). The median ages for arms A and B were 56 and 54 years, respectively. Total numbers for AA and GBM patients were 15 (27.3 %) and 40 (72.7 %) in arm A and 15 (26.8 %) and 41 (73.2 %) in arm B. PS 0 to 1 in arms A and B were 45 (81.8 %) and 41 (73.2 %), respectively. Eighteen (32.7 %) patients in arm A and 21 (37.5 %) patients in arm B underwent gross total removal, and no residual tumor was confirmed on MRI scans. The median duration of follow-up was 20.2 (range 0–48.0 months) for all eligible patients.

Treatment

Patient compliance with the treatment regimen is depicted in Table 2. Among the 111 total patients, 1 patient in arm A died from pulmonary embolism before the beginning of initial chemoradiotherapy. Fifty-three (96.3 %) patients in arm A completed initial chemoradiotherapy and received ACNU twice. In arm B, 48 out of 56 (85.7 %) patients received 2 cycles of PCZ + ACNU, and 8 patients (14.3 %) received 1 cycle of PCZ + ACNU in initial chemoradiotherapy. Eighteen (32.7 %) patients in arm A and 20 (35.7 %) patients in arm B failed to start adjuvant chemotherapy. Furthermore, 14 (25.5 %) patients in arm A and 23 (41.1 %) patients in arm B discontinued protocol therapy by the fourth cycle of adjuvant chemotherapy. The numbers of patients who received 4 cycles of chemotherapy or more were 23 (41.8 %) and 13 (23.2 %) in arm A and B, respectively. Only 5 (9.1 %) patients in arm A and 2 (3.6 %) patients in arm B completed the full protocol therapy. Nineteen (34.5 %) patients in arm A and 22 (39.3 %) patients in arm B discontinued the protocol for reasons other than completion of protocol or disease progression [arm A: 31 (56.4 %), arm B: 32 (57.1 %)]. Reasons for discontinuation were as follows: AEs [arm A: 6 (10.9 %), arm B: 13 (23.2 %)]; patient refusal related to AE

Table 1 Baseline characteristics in the ITT population

	Arm A ($n = 55$) (RT + ACNU)	Arm B ($n = 56$) (RT + PCZ + ACNU)
Age	56 (24–69)	54 (24–69)
Sex		
Male	32 (58.2 %)	33 (58.9 %)
Female	23 (41.8 %)	23 (41.1 %)
PS		
0, 1	45 (81.8 %)	41 (73.2 %)
2, 3	10 (18.2 %)	15 (26.8 %)
Histology		
Grade 3 (AA)	15 (27.3 %)	15 (26.8 %)
Grade 4 (GBM)	40 (72.7 %)	41 (73.2 %)
Surgery		
Gross total removal	18 (32.7 %)	21 (37.5 %)
Partial removal	30 (54.5 %)	26 (46.4 %)
Biopsy only	7 (12.7′ %)	9 (16.1 %)

Table 2 Compliance

	Arm A ($n = 55$) (RT + ACNU)	Arm B ($n = 56$) (RT + PCZ + ACNU)
RT (completion)	54 (98.2 %)	56 (100 %)
Initial chemotherapy		
1 cycle	1 (1.8 %)	8 (14.3 %)
2 cycles	53 (96.4 %)	48 (85.7 %)
Adjuvant chemotherapy		
None	18 (32.7 %)	20 (35.7 %)
1–3 cycles	14 (25.5 %)	23 (41.1 %)
4–6 cycles	9 (16.4 %)	7 (12.5 %)
7–11 cycles	9 (16.4 %)	4 (7.1 %)
12 cycles (completion)	5 (9.1 %)	2 (3.6 %)

[arm A: 3 (5.5 %), arm B: 8 (14.3 %)]; and patient refusal not related to AE [arm A: 7 (12.7 %), arm B: 1 (1.8 %)].

After discontinuation of the protocol, 28 (50.9 %) patients in arm A and 29 (51.8 %) patients in arm B received TMZ as further treatment.

Central review of histology

The central pathology review diagnosis of all cases was performed according to the WHO 2007 classification (Table 3). Among 81 GBM in the intention-to-treat (ITT) population, 69 (85.2 %), 4 (4.9 %), 3 (3.7 %), 2 (2.5 %), and 3 (3.7 %) were diagnosed as GBM, anaplastic oligoastrocytoma (AOA), anaplastic oligodendroglioma (AO), AA, and others, respectively. Only 10 cases (33.3 %) were diagnosed as AA among the 30 AA in the ITT population, while 8 (26.7 %), 5 (16.7 %), 3 (10.0 %), 2 (6.7 %), and 2 (6.7 %) were confirmed as GBM, AOA, diffuse astrocytoma, pilocytic astrocytoma, and others, respectively. Among all 111 cases, phenotype change of astrocytic to oligodendroglial tumor occurred in 14 cases (12.6 %). Finally, 77 and 12 patients were diagnosed with GBM and AA, respectively, by central pathology review.

Response rate

The overall radiographic response rate for 66 measurable diseases after surgery, based on RECIST guideline, was assessed by Diagnostic Radiology Committee. The response rate was 21.2 % (7/33) in arm A and 6.1 % (2/33) in arm B. In GBM patients from the ITT population, response rates were 25.0 % in arm A [3 CR (complete response), 2 PR (partial response), 1 SD (stable disease), 14 PD (progressive disease)] and 9.1 % in arm B [1 CR, 1 PR, 1 SD, 19 PD] ($p = 0.23$). In AA patients from the ITT population, response rates were 15.4 % in arm A (2 PR, 1 SD, 10 PD) and 0 % in arm B (11 PD) ($p = 0.48$).

Progression-free survival

In the entire ITT population, PFS was 8.6 months [95 % confidence interval (CI); 5.1–20.5] in arm A ($n = 55$, 44 events), compared with 6.9 months (95 % CI 5.1–9.0, $p = 0.36$) in arm B ($n = 56$, 47 events) (Fig. 2a). According to grades in the ITT population, PFS of GBM in arm A ($n = 40$, 33 events) and B ($n = 41$, 35 events) was 6.2 (95 % CI 4.2–13.2) and 6.3 months (95 % CI 3.0–8.9), respectively ($p = 0.35$) (Fig. 2b). PFS of AA in arm A ($n = 15$, 11 PD) and B ($n = 15$, 12 events) was 8.6 (95 % CI 5.1–35.4) and 9.0 months (95 % CI 5.8–21.8), respectively ($p = 0.83$) (Fig. 2c). No difference was observed between the arms in any subgroup defined by histology, presence of remaining tumor, or age under or over 60.

In the subgroup defined by central pathology review, the PFS of GBM in arms A ($n = 37$, 33 events) and B ($n = 40$, 36 events) was 5.1 (95 % CI 4.2–10.3) and 5.7 months (95 % CI 2.7–8.4), respectively ($p = 0.49$) (Fig. 2d). The PFS of AA and AOA in arm A ($n = 9$, 4 events) and B ($n = 12$, 9 events) was ND (not determined) and 7.9 months (95 % CI 5.2–22.5), respectively ($p = 0.21$).

Table 3 Local diagnosis and central pathology review

Grade	Histology	Local diagnosis	Central pathology review		
			Total	Arm A	Arm B
IV	*Glioblastoma*	83	77	37	40
III	*Anaplastic astrocytoma*	30	12	6	6
III	Anaplastic oligoastrocytoma		9	3	6
III	Anaplastic oligodendroglioma		3	2	1
III	Anaplastic ependymoma		1	1	0
II	Diffuse astrocytoma		4	1	3
II	Oligoastrocytoma		1	1	0
II	Oligodendroglioma		1	1	0
I	Pilocytic astrocytoma		2	2	0
	Sarcoma		1	1	0
	Total	111	111	55	56

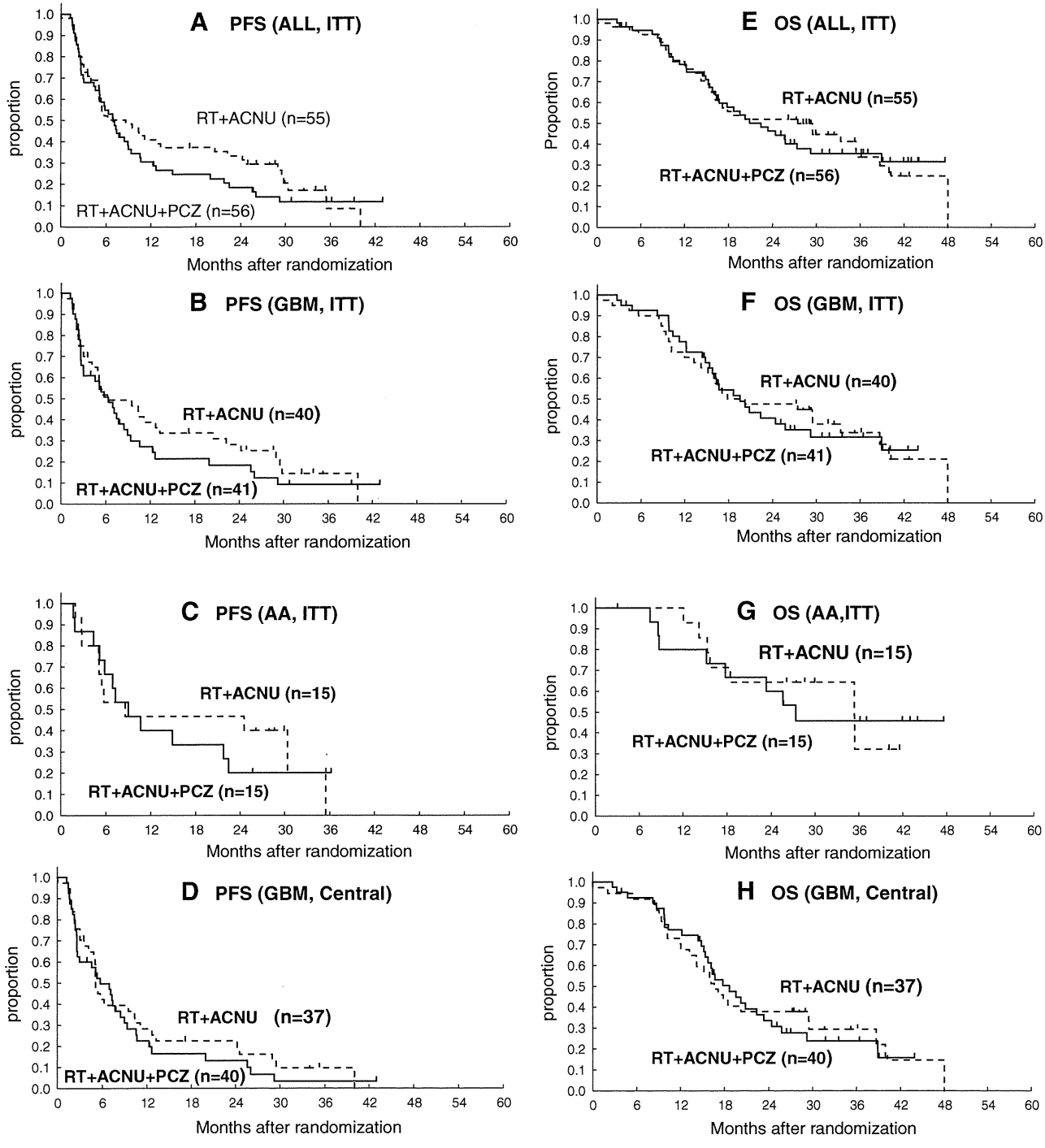

Fig. 2 Progression-free survival in the intention-to-treat (ITT) population (**a**), the GBM subgroup (**b**), the AA subgroup (**c**), and the GBM subgroup with central pathology review (**d**). Overall survival in the ITT population (**e**), the GBM subgroup (**f**), the AA subgroup (**g**), and the GBM subgroup with central pathology review (**h**). RT + ACNU alone (*solid line*), RT + ACNU + PCZ (*dotted line*)

Overall survival and cause of death

From the entire ITT population, 35 patients died in each group. In arm A ($n = 55$), OS was 27.4 months (95 % CI 16.2–35.4), compared with 22.4 months (95 % CI 16.4–29.2) in arm B ($n = 56$) (Fig. 2e). The %2-year survival in arms A and B was 51.9 % and 46.2 %, respectively. There was no difference between the 2 arms ($p = 0.75$ and pre-planned, one-sided $p = 0.62$, by stratified log-rank test).

The OS of GBM subgroup in arms A ($n = 40$, 28 death) and B ($n = 41$, 27 death) was 19.0 (95 % CI 15.2–33.3) and 19.5 months (95 % CI 15.8–29.2), respectively ($p = 0.90$) (Fig. 2f). The %2-year survival in arms A and B was 48 and 41 %, respectively. The OS of AA subgroup in arms A ($n = 15$, 7 death) and in arm B ($n = 15$, 8 death) was 35.4 [95 % CI 15.7–not estimated (NE)] and 27.4 months (95 % CI 17.8–NE), respectively ($p = 0.88$) (Fig. 2g). There were no differences between the arms of any subgroup.

In the subgroups defined by central pathology review, the OS of GBM in arm A ($n = 37$, 28 death) and in arm B ($n = 40$, 29 death) was 16.6 (95 % CI 13.3–29.5) and 18.7 months (95 % CI 15.4–23.4), respectively ($p = 0.92$) (Fig. 2h). The %2-year survival in arms A and B was 38 and 34 %, respectively. The OS of AA and AOA in arm A ($n = 9$, 3 death) and B ($n = 12$, 4 death) was 33.3 months (95 % CI 15.7–33.3) and NE, respectively ($p = 0.83$).

Among the 70 total deaths, 31/35 (88.6 %) patients in arm A and 32/35 (91.4 %) in arm B experienced neuronal death of an original tumor. One patient (2.9 %) in arm A and 2 (5.7 %) patients in arm B contracted treatment-related pneumonia and died from that illness. Other causes of death were pulmonary embolism (1), pneumonia (2), and unknown (1).

Toxicity

Toxicity was assessed in 110 patients receiving initial therapy and in 73 patients receiving adjuvant chemotherapy. The most frequent grade 3/4 toxicities, experienced by more than 10 % of patients, were hematologic, neurologic, gastrointestinal, and hepatic AEs (Table 4). Patients in both arms frequently experienced leukopenia and neutropenia; more than half of the patients in arm B experienced these AEs during adjuvant therapy as well as during initial therapy. More than 40 % of patients in arm A also experienced these hematologic events even during adjuvant therapy. Grade 4 neutropenia was observed in 5.6 and 39.3 % of patients in arms A and B during initial chemoradiotherapy and 11.1 and 15.6 % during adjuvant therapy. Grade 3/4 nausea and anorexia were seen in 10.7 and 16.1 % of patients in initial therapy in arm B, but were rare in the adjuvant-therapy subgroups in both arms. One patient in arm B had cerebral infarction. Extrapyramidal signs, including tremors or involuntary movements, occurred in 2 patients in each arm.

Grade 3/4 pneumonitis occurred in 1 patient in arm A and 2 in arm B during the entire treatment period. Opportunistic infections—including 2 cases of *Pneumocystis jirovecii* pneumonia (PCP), 1 case of oral candidiasis, and 2 case of herpes zoster—occurred in arm B. One patient (1.8 %) in arm A and 2 (3.6 %) patients in arm B died from treatment-related pneumonia, and 1 of these patients in arm B had PCP. One patient in arm B died from sepsis and acute respiratory distress syndrome after initial therapy. One patient in arm A died from pulmonary embolism before starting chemoradiotherapy, and 1 patient in arm A and 2 patients in arm B died from pneumonia following tumor progression.

Radiation necrosis was observed in 2 out of 54 (3.7 %) patients in arm A and 1 out of 56 (1.8 %) patients in arm B. During surgery, 1 patient in arm A was found to have radiation necrosis. Pseudo-progression within 3 months after chemoradiotherapy was not suspected in any patient.

Discussion

This study aimed to evaluate the efficacy and safety of treatment with ACNU + PCZ compared to ACNU alone as concomitant chemoradiotherapy against AA and GBM. We found no obvious differences in OS or PFS for AA and GBM between the treatment groups, but patients treated with ACNU + PCZ experienced more adverse effects than those treated with ACNU alone. TMZ is an effective regimen for malignant gliomas with less toxicity than our ACNU regimens, but it was not approved in Japan when this study began. At the end of the phase II part of this study, TMZ became available even in Japan, so this study was terminated at that point.

Methylguanine DNA methyltransferase is a major DNA repair protein and is implicated in resistance of glioma cells to alkylating agents [13]. Transcriptional silencing by MGMT promoter methylation results in inhibition of MGMT expression [14], and thus MGMT promoter methylation is strongly associated with survival in glioma patients treated with either nitrosourea or TMZ [15–17]. The status of the promoter of MGMT in primary tumors was frequently observed to change from methylated to unmethylated in recurrent tumors following ACNU or TMZ treatment [18, 19], which constitutes one of the mechanisms behind malignant gliomas' resistance to nitrosourea and TMZ. The rationale for treatment with ACNU + PCZ is that daily application of PCZ depletes MGMT activity, increasing sensitivity of AA and GBM to ACNU. Dose-dense TMZ therapy based on the theory of depletion of MGMT [20, 21], or BCNU or TMZ with direct inhibition of MGMT by O^6-benzylguanine [22, 23] has been shown in previous studies to be effective for GBMs. However, there was no difference in OS found between standard and dose-dense TMZ for newly diagnosed GBMs [20].

While we were conducting this study, the European Organization for Research and Treatment of Cancer (EORTC) Brain Tumor and Radiotherapy Groups and the

Table 4 Toxicity

Grade 3/4 adverse events	Initial therapy with RT (n = 110) (%)		Adjuvant therapy (n = 73) (%)	
	Arm A	Arm B	Arm A	Arm B
Hematologic				
Leukopenia	38.9	73.2	40.5	69.4
Neutropenia	38.9	76.8	44.4	56.3
Thrombocytopenia	5.6	50.0	40.5	50.0
Anemia	0	8.9	10.8	8.3
Neurologic				
Seizure	9.3	7.1	5.4	8.8
Speech impairment	11.1	10.7	5.4	2.9
Neuropathy-motor	11.1	12.5	0	0
Extrapyramidal sign	0	0	5.4	2.7
Pulmonary (pneumonitis)	0	3.6	2.7	0
Gastrointestinal				
Nausea	0	10.7	0	0
Anorexia	1.9	16.1	0	2.9
Hepatic				
AST	3.7	12.5	2.9	2.9
ALT	3.7	16.1	2.9	8.8
Total bilirubin	1.9	5.4	0	0
Renal (creatinine)	0	0	0	0
Metabolic				
Hyponatremia	1.9	8.9	5.9	2.9
Hypokalemia	1.9	7.1	2.9	2.9
Fever	0	3.6	0	0
Dermatologic: erythema	3.7	5.4	0	2.9

National Cancer Institute of Canada (NCIC) Clinical Trials Group (EORTC/NCIC TMZ study) reported, in 2005, that RT + TMZ significantly prolonged the survival of GBM patients compared to RT alone [24]. The median PFS, OS, and 2-year survival for RT + TMZ were 6.9, 14.6 months, and 26.5 %, respectively [24]. Although our results compared favorably with the EORTC/NCIC TMZ study, the PFS of RT + ACNU alone for GBMs in our ITT population and in GBM subgroups in central pathology review were 6.2 and 5.1 months, shorter than those from the EORTC/NCIC TMZ study. Since more than half of the patients in our study underwent TMZ treatment following disease progression, it is possible that TMZ rescued these patients with progression after ACNU regimens and prolonged the survival of these patients.

The incidence of grade 3/4 hematologic AEs—such as leukopenia, neutropenia, and thrombocytopenia—were reported to be 5, 4, and 11 %, respectively, in adjuvant TMZ therapy in the EORTC/NCIC TMZ trial [24]. Compared to TMZ, even ACNU alone caused severe hematologic AEs in 40 % of the patients in our study, and most of those patients in both arms discontinued the treatment protocol due to AEs or patient refusal related to AEs. It is noteworthy that approximately 30 % of patients in both arms failed to start adjuvant chemotherapy. The low completion rate of our protocol might explain the lack of differences in PFS and OS between the arms. After 2 patients in arm B experienced PCP, prophylactic use of cotrimoxazole (trimethoprim–sulfamethoxazole) against PCP was recommended in this study and was found to be useful.

Radiation necrosis has been reported in 2.5–21 % of patients undergoing chemoradiotherapy against malignant gliomas [25]. This complication was observed in 2.7 % of the patients in our study, but was tolerable. "Pseudo-progression" is the phenomenon of transient early disease progression after treatment with chemoradiotherapy consisting of TMZ for GBM progressive and enhancing lesions, as shown on MRI images taken immediately after treatment [25]. No patients in our study were suspected of pseudo-progression within 6 months after beginning chemoradiotherapy.

In general, the difference in histological diagnosis for local versus central pathology review is a major problem in the conduct of clinical trials on gliomas [26]. In our study, the concordance of GBM and AA between local and central diagnosis was low, but nearly identical to previous reports. In the EORTC/NCIC TMZ trial, central pathology review was performed in 85 % of cases, which confirmed the diagnosis of GBM in 93 % of the reviewed cases; 3 % had AA or AOA. In the phase III study of RT versus RT + BCNU + dibromodulcitol (EORTC 26882), of the 193 cases of AA diagnosed by the local pathologist, 176 were reviewed by the central pathologist. At review, 61 patients (35 %) were diagnosed with AA, 13 (8 %) with AOA, 4 (2 %) with AO, 44 (25 %) with GBM, 41 (23 %) with low-grade gliomas, and 13 (7 %) with another diagnosis [27].

The WHO classification system reflects the prognoses depending on grade I–IV tumors, or astrocytic or oligodendroglial tumors. However, it is based on morphological descriptions and contains subjective elements; thus, inter-observer variation occurs. The boundaries between grades II, III, and IV in gliomas are unclear, and there is a trend toward a more frequent diagnosis of oligodendroglial tumors [28]. Central pathological review before inclusion of a patient into clinical study is ideal, but it is very difficult to complete for aggressive grade III/IV tumors. Even if central review before enrollment is difficult in a multi-institutional setting, it is indispensable to perform post hoc central review at least in order to appropriately interpret the results of clinical studies of gliomas. A consensus meeting might also be useful before commencing clinical studies in order to gain concordance between local and central diagnoses. More objective classification of tumors based on

genotype, such the IDH1/2 mutation or 1p/19q codeletion, should be included in at least the stratification factor and subgroup analysis.

Conclusions

No significant differences in OS or PFS were found between ACNU alone and ACNU + PCZ in either AA or GBM. We found that ACNU + PCZ treatment was more toxic in our treatment schedule. Therefore, we conclude that the addition of PCZ to ACNU was not beneficial for newly diagnosed, high-grade astrocytomas as compared to ACNU alone. Considering the greater number of AEs associated with ACNU regimens, RT + TMZ should serve as a standard therapeutic regimen in the treatment of newly diagnosed AA and GBM.

Acknowledgments We thank all the members of the JCOG Brain Tumor Study Group and the staff of the JCOG Data Center. We appreciate Dr. Nobuaki Funata and Dr. Toru Iwaki for pathological review, Dr. Satoshi Ishikura for quality assurance of radiation therapy, and Dr. Hiroshi Katayama, Dr. Kenichi Nakamura, and Mr. Hidenobu Yamada for review of the manuscript. This work was supported in part by the National Cancer Center Research and Development Fund (23A-16 and 23A-20), the Health and Labour Sciences Research Grants (H14-032, H15-025, H16-005, H17-005), and the Grant-in Aid for Cancer Research (20S-4, 20S-6) from the Ministry of Health, Labour and Welfare.

Conflict of interest The authors declare that they have no conflict of interest.

References

1. The Committee of Brain Tumor Registry of Japan (2003) Report of brain tumor registry of japan (1984–2000) 12th edition. Neurol Med Chir (Tokyo) 49(Suppl):1–101
2. Glioma Meta-analysis Trialists (GMT) Group (2002) Chemotherapy in adult high-grade glioma: a systematic review and meta-analysis of individual patient data from 12 randomised trials. Lancet 359(9311):1011–1018. doi:10.1016/S0140-6736(02)08091-1
3. Matsutani M, Nakamura O, Nakamura M, Nagashima T, Asai A, Fujimaki T, Tanaka H, Ueki K, Tanaka Y (1994) Radiation therapy combined with radiosensitizing agents for cerebral glioblastoma in adults. J Neurooncol 19(3):227–237
4. Wolff JE, Berrak S, Koontz Webb SE, Zhang M (2008) Nitrosourea efficacy in high-grade glioma: a survival gain analysis summarizing 504 cohorts with 24193 patients. J Neurooncol 88(1):57–63. doi:10.1007/s11060-008-9533-5
5. Takakura K, Abe H, Tanaka R, Kitamura K, Miwa T, Takeuchi K, Yamamoto S, Kageyama N, Handa H, Mogami H et al (1986) Effects of ACNU and radiotherapy on malignant glioma. J Neurosurg 64(1):53–57. doi:10.3171/jns.1986.64.1.0053
6. Pegg AE (1990) Mammalian O^6-alkylguanine-DNA alkyltransferase: regulation and importance in response to alkylating carcinogenic and therapeutic agents. Cancer Res 50(19):6119–6129
7. Silber JR, Bobola MS, Ghatan S, Blank A, Kolstoe DD, Berger MS (1998) O^6-methylguanine-DNA methyltransferase activity in adult gliomas: relation to patient and tumor characteristics. Cancer Res 58(5):1068–1073
8. Valavanis C, Souliotis VL, Kyrtopoulos SA (1994) Differential effects of procarbazine and methylnitrosourea on the accumulation of O^6-methylguanine and the depletion and recovery of O^6-alkylguanine-DNA alkyltransferase in rat tissues. Carcinogenesis 15(8):1681–1688
9. Souliotis VL, Kaila S, Boussiotis VA, Pangalis GA, Kyrtopoulos SA (1990) Accumulation of O^6-methylguanine in human blood leukocyte DNA during exposure to procarbazine and its relationships with dose and repair. Cancer Res 50(9):2759–2764
10. Wedge SR, Porteus JK, May BL, Newlands ES (1996) Potentiation of temozolomide and BCNU cytotoxicity by O(6)-benzylguanine: a comparative study in vitro. Br J Cancer 73(4):482–490
11. Therasse P, Arbuck SG, Eisenhauer EA, Wanders J, Kaplan RS, Rubinstein L, Verweij J, Van Glabbeke M, van Oosterom AT, Christian MC, Gwyther SG (2000) New guidelines to evaluate the response to treatment in solid tumors. European Organization for Research and Treatment of Cancer, National Cancer Institute of the United States, National Cancer Institute of Canada. J Natl Cancer Inst 92(3):205–216
12. Bernstein D, Lagakos SW (1978) Sample size and power determination for stratified clinical trials. J Stat Comput Simul 8:65–73
13. Bobola MS, Tseng SH, Blank A, Berger MS, Silber JR (1996) Role of O^6-methylguanine-DNA methyltransferase in resistance of human brain tumor cell lines to the clinically relevant methylating agents temozolomide and streptozotocin. Clin Cancer Res 2(4):735–741
14. Esteller M, Garcia-Foncillas J, Andion E, Goodman SN, Hidalgo OF, Vanaclocha V, Baylin SB, Herman JG (2000) Inactivation of the DNA-repair gene MGMT and the clinical response of gliomas to alkylating agents. N Engl J Med 343(19):1350–1354. doi:10.1056/NEJM200011093431901
15. Hegi ME, Diserens AC, Gorlia T, Hamou MF, de Tribolet N, Weller M, Kros JM, Hainfellner JA, Mason W, Mariani L, Bromberg JE, Hau P, Mirimanoff RO, Cairncross JG, Janzer RC, Stupp R (2005) MGMT gene silencing and benefit from temozolomide in glioblastoma. N Engl J Med 352(10):997–1003. doi:10.1056/NEJMoa043331
16. Sonoda Y, Yokosawa M, Saito R, Kanamori M, Yamashita Y, Kumabe T, Watanabe M, Tominaga T (2010) O(6)-Methylguanine DNA methyltransferase determined by promoter hypermethylation and immunohistochemical expression is correlated with progression-free survival in patients with glioblastoma. Int J Clin Oncol 15(4):352–358. doi:10.1007/s10147-010-0065-6
17. van den Bent MJ, Gravendeel LA, Gorlia T, Kros JM, Lapre L, Wesseling P, Teepen JL, Idbaih A, Sanson M, Smitt PA, French PJ (2011) A hypermethylated phenotype is a better predictor of survival than MGMT methylation in anaplastic oligodendroglial brain tumors: a report from EORTC study 26951. Clin Cancer Res 17(22):7148–7155. doi:10.1158/1078-0432.CCR-11-1274
18. Brandes AA, Franceschi E, Tosoni A, Bartolini S, Bacci A, Agati R, Ghimenton C, Turazzi S, Talacchi A, Skrap M, Marucci G, Volpin L, Morandi L, Pizzolitto S, Gardiman M, Andreoli A, Calbucci F, Ermani M (2010) O(6)-methylguanine DNA-methyltransferase methylation status can change between first surgery for newly diagnosed glioblastoma and second surgery for recurrence: clinical implications. Neuro Oncol 12(3):283–288. doi:10.1093/neuonc/nop050
19. Okita Y, Narita Y, Miyakita Y, Ohno M, Fukushima S, Kayama T, Shibui S (2012) Pathological findings and prognostic factors in recurrent glioblastomas. Brain Tumor Pathol. doi:10.1007/s10014-012-0084-2
20. Aldape KD, Wang M, Sulman EP, Hegi M, Colman H, Jones G, Chakravarti A, Mehta MP, Andrews DW, Long L, Diefes K,

Heathcock L, Jenkins R, Schultz CJ, Gilbert MR, Group RTO (2011) RTOG 0525: Molecular correlates from a randomized phase III trial of newly diagnosed glioblastoma. ASCO Annu Meet Proc 29(18_suppl):LBA2000

21. Wick A, Felsberg J, Steinbach JP, Herrlinger U, Platten M, Blaschke B, Meyermann R, Reifenberger G, Weller M, Wick W (2007) Efficacy and tolerability of temozolomide in an alternating weekly regimen in patients with recurrent glioma. J Clin Oncol 25(22):3357–3361. doi:10.1200/JCO.2007.10.7722
22. Quinn JA, Jiang SX, Reardon DA, Desjardins A, Vredenburgh JJ, Rich JN, Gururangan S, Friedman AH, Bigner DD, Sampson JH, McLendon RE, Herndon JE 2nd, Walker A, Friedman HS (2009) Phase II trial of temozolomide plus O^6-benzylguanine in adults with recurrent, temozolomide-resistant malignant glioma. J Clin Oncol 27(8):1262–1267. doi:10.1200/JCO.2008.18.8417
23. Quinn JA, Pluda J, Dolan ME, Delaney S, Kaplan R, Rich JN, Friedman AH, Reardon DA, Sampson JH, Colvin OM, Haglund MM, Pegg AE, Moschel RC, McLendon RE, Provenzale JM, Gururangan S, Tourt-Uhlig S, Herndon JE 2nd, Bigner DD, Friedman HS (2002) Phase II trial of carmustine plus O(6)-benzylguanine for patients with nitrosourea-resistant recurrent or progressive malignant glioma. J Clin Oncol 20(9):2277–2283
24. Stupp R, Mason WP, van den Bent MJ, Weller M, Fisher B, Taphoorn MJ, Belanger K, Brandes AA, Marosi C, Bogdahn U, Curschmann J, Janzer RC, Ludwin SK, Gorlia T, Allgeier A, Lacombe D, Cairncross JG, Eisenhauer E, Mirimanoff RO (2005) Radiotherapy plus concomitant and adjuvant temozolomide for glioblastoma. N Engl J Med 352(10):987–996
25. Brandes AA, Tosoni A, Spagnolli F, Frezza G, Leonardi M, Calbucci F, Franceschi E (2008) Disease progression or pseudoprogression after concomitant radiochemotherapy treatment: pitfalls in neurooncology. Neuro Oncol 10(3):361–367. doi:10.1215/15228517-2008-008
26. van den Bent MJ (2010) Interobserver variation of the histopathological diagnosis in clinical trials on glioma: a clinician's perspective. Acta Neuropathol 120(3):297–304. doi:10.1007/s00401-010-0725-7
27. Hildebrand J, Gorlia T, Kros JM, Afra D, Frenay M, Omuro A, Stupp R, Lacombe D, Allgeier A, van den Bent MJ (2008) Adjuvant dibromodulcitol and BCNU chemotherapy in anaplastic astrocytoma: results of a randomised European Organisation for Research and Treatment of Cancer phase III study (EORTC study 26882). Eur J Cancer 44(9):1210–1216. doi:10.1016/j.ejca.2007.12.005
28. Coons SW, Johnson PC, Scheithauer BW, Yates AJ, Pearl DK (1997) Improving diagnostic accuracy and interobserver concordance in the classification and grading of primary gliomas. Cancer 79(7):1381–1393

Japanese Journal of Clinical Oncology Advance Access published April 12, 2013

JJCO Japanese Journal of Clinical Oncology

Jpn J Clin Oncol 2013
doi:10.1093/jjco/hyt051

Review Article

Drug Review: Safety and Efficacy of Bevacizumab for Glioblastoma and Other Brain Tumors

Yoshitaka Narita*

Department of Neurosurgery and Neuro-Oncology, National Cancer Center Hospital, Tokyo, Japan

*For reprints and all correspondence: Yoshitaka Narita, Department of Neurosurgery and Neuro-Oncology, National Cancer Center Hospital, 5-1-1, Tsukiji, Chuo-ku, Tokyo 104-0045, Japan. E-mail: yonarita@ncc.go.jp

Received January 21, 2013; accepted March 14, 2013

Glioblastoma is a highly vascular tumor that expresses vascular endothelial growth factor, a key regulator of angiogenesis and tumor blood vessel permeability. Bevacizumab is a monoclonal antibody that inhibits vascular endothelial growth factor and the growth of gliomas. Bevacizumab monotherapy has proven effective for recurrent glioblastoma, and it extended progression-free survival and improved patient quality of life in various clinical trials. Some patients who receive bevacizumab experience improvements in neurological symptoms and steroid dose reductions. Bevacizumab induces a dramatic and rapid radiological response, but non-enhancing lesions are often detected on magnetic resonance imaging without enhancing lesions. Rebound phenomena such as rapid tumor regrowth are occasionally observed after the discontinuation of bevacizumab therapy. Therefore, Response Assessment in Neuro-Oncology criteria were recently devised to evaluate the efficacy and radiological response of bevacizumab treatment. Hypertension and proteinuria are characteristic adverse events associated with bevacizumab therapy. In addition, many fatal adverse events such as intracranial hemorrhage and venous thromboembolism are reported in patients treated with bevacizumab. However, these events are also associated with glioma itself, and careful attention needs to be paid to these events. Bevacizumab is used to treat various diseases including radiation necrosis and recurrent brain tumors such as brain metastases, schwannoma and meningioma, but additional clinical trials are necessary. The efficacy and current problems associated with bevacizumab in the treatment of glioblastoma and other brain tumors are reviewed.

Key words: bevacizumab – glioblastoma – glioma – brain metastases – rebound

INTRODUCTION

Glioblastoma (GBM), the most common malignant brain tumor, is associated with a survival time of 1–2 years. The standard therapy for a newly diagnosed GBM is maximum resection in patients without neurological deficits and radiotherapy (RT) plus the alkylating agent temozolomide (TMZ) (1). GBM is a highly vascular tumor, and an alternative therapeutic approach that inhibits angiogenesis is expected to inhibit the growth of GBM.

Vascular endothelial growth factor (VEGF), a key regulator of angiogenesis, is highly expressed in GBM (2–4). The expression of VEGF correlates with the grade of gliomas (5), and VEGF expression is also observed in meningioma and brain metastases (3). The molecular bases for the upregulation of VEGF gene expression in gliomas are as follows: (i) hypoxia or the hypoxia inducible factor (HIF)-related mechanism, (ii) epidermal growth factor receptor signaling, (iii) upregulation of the Forkhead box M1B (FoxM1B) transcription factor in GBM but not in low-grade glioma, which stimulates VEGF expression independently of HIF and (iv) upregulation of HuR, a member of the Elav family of RNA-binding proteins, in GBM, which suppresses the post-

transcriptional degradation of VEGF mRNA under hypoxia (6). VEGF signaling regulates angiogenesis and tumor blood vessel permeability, which promote endothelial cell proliferation, survival and migration and cerebral edema (6).

Monoclonal antibodies against VEGF have been demonstrated to inhibit the growth of GBM xenografts in an *in vivo* mouse model (7,8). Bevacizumab (Avastin®), a monoclonal antibody that inhibits the VEGF, is currently approved for metastatic colorectal, non-small-cell lung, breast, ovarian and renal cancers. Based on the results of many clinical trials of bevacizumab for the treatment of GBM, bevacizumab is currently recognized as a second-line chemotherapeutic agent for GBM. The application of bevacizumab for recurrent GBM is also described in the National Comprehensive Cancer Network guideline (9), and it has been approved in more than 41 countries. This article reviews the efficacy and current problems of bevacizumab therapy against GBM and other brain tumors.

RECURRENT GBM

Bevacizumab is a standard therapeutic agent for recurrent GBM or WHO grade III malignant gliomas after treatment with RT plus TMZ, and no other effective therapy is available. Single-agent bevacizumab after the failure of initial treatment with mainly TMZ for malignant gliomas has a reported objective response rate (ORR), progression-free survival (PFS), 6-month PFS rate and overall survival (OS) of 20.9–42.6%, 1.0–4.2 months, 20.9–42.6% and 7.1–12 months, respectively, as calculated from the initiation of bevacizumab treatment (10–14) (Table 1).

Bevacizumab alone or in combination with irinotecan was similarly effective for recurrent GBM in the BRAIN study (11). The PFS times were 4.2 and 5.6 months in the bevacizumab alone ($n = 85$) and bevacizumab plus irinotecan ($n = 87$) groups, respectively, and the OS times were 9.2 and 8.7 months, respectively, in the two groups. The 6-month PFS rates for bevacizumab alone and bevacizumab plus irinotecan were 42.6 and 50.3%, respectively, and the ORRs were 28.2 and 37.8%, respectively, for the two treatments. Based on these results, the US Food and Drug Administration (FDA) first granted bevacizumab accelerated approval for the treatment of recurrent GBM in 2009 (15).

Table 1. Efficacy of single-agent bevacizumab for malignant gliomas

Study	ORR (%)	PFS	6-month PFS rate (%)	OS from bevacizumab
BRAIN, 2009	28.2	4.2	42.6	9.2
JO22506, 2012	27.6	3.3	33.9	10.5
Kreisl, 2009	35	3.7	29	7.1
Chamberlain, 2010	42	1.0	42	8.5
Kreisl, 2010	43	2.9	20.9	12

ORR; overall response rate, PFS; progression-free survival, OS; overall survival.

The JO22506 study in Japan also revealed that single-agent bevacizumab was effective for recurrent malignant gliomas ($n = 31$) (14). The PFS and OS were 3.3 and 10.5 months, respectively, for this treatment. Additionally, the 6-month PFS rate, ORR and disease control rate were 33.9, 27.6, and 79.3%, respectively, and these findings were comparable with those of the BRAIN study. Approximately 70% of patients who received corticosteroids before treatment were able to reduce their dose or discontinue corticosteroid therapy after bevacizumab treatment, and >70% of patients displayed a lower tumor volume on magnetic resonance imaging (MRI) 6 weeks after treatment in this study.

Combination therapy of bevacizumab and irinotecan (11,12,16–18), carboplatin (19–21), erlotinib (22), etoposide (23) and dose-intense daily TMZ (24,25) for malignant gliomas was reported, and the treatment results were similar to that of single-agent bevacizumab therapy.

Generally, the 6-month PFS rate and OS of recurrent GBM are 10–20% and ~6 months, respectively (26–28). Thus, single-agent bevacizumab has become the most promising second-line agent for recurrent GBM in adult. However, there are a few reports about the use of bevacizumab to treat recurrent pediatric high-grade gliomas or brainstem gliomas, and the radiological response rate, response duration and survival of children appeared to be inferior to those of adult cases (29–32).

Marked decreases in enhancing lesions and surrounding cerebral edema have been observed after the initiation of therapy, and patients exhibited improvements in clinical symptoms. Approximately 30–70% of patients who received bevacizumab could reduce their steroid doses (14,33). Steroids have been used to treat patients with brain tumors to control brain edema, and bevacizumab is occasionally considered an 'expensive super steroid'. Thus, patients treated with bevacizumab display improved quality of life due to improvements in clinical symptoms and reductions of steroid doses, even if for a short time.

Wong et al. performed a meta-analysis of bevacizumab for recurrent GBM in 548 patients from 15 studies and reported that the 6-month PFS rate and OS were 45% and 9.3 months, respectively. The treatment doses of bevacizumab in most clinical trials were 10 mg/kg every 2 weeks, but they reported no difference in the bevacizumab dose response benefit between doses of 5 mg/kg and 10–15 mg/kg (34). The efficacy of superselective intra-arterial cerebral infusion of bevacizumab to increase the local concentration of the drug around the tumor has been reported (35).

MRI FINDINGS AFTER BEVACIZUMAB TREATMENT

Bevacizumab exhibited a dramatic and rapid reducing effect on enhancing lesions on MRI (36,37), and >70% patients

displayed smaller enhancing lesions 6 weeks after the initiation of treatment (14). However, this effect is not caused by the antitumor effect of bevacizumab, but is attributable to the normalization of abnormally permeable tumor vessels or regional cerebral blood volume (38). Non-enhancing lesions on T2 or fluid-attenuated inversion recovery MRI are often detected without enhancing lesions, which are indicative of progressive infiltrative tumors. Iwamoto et al. reported that 46% of patients had larger enhancing lesions at the initial tumor site, 16% had a new enhancing lesion outside the initial site, and 35% had progression of predominantly non-enhancing tumors at the time of bevacizumab discontinuation for recurrent GBM (36).

The Macdonald criteria have been used for response assessment in glioma (39). These criteria are based on the two-dimensional WHO response criteria, and they use the enhancing tumor area on computed tomography (CT) or MRI as the primary measure while considering the use of steroids and changes in the neurologic status. However, these criteria cannot evaluate the enlargement of the non-enhancing area upon bevacizumab treatment or a pseudoresponse, which is often visualized as a transient increase in the enhancing lesion in patients receiving TMZ treatment. Thus, the Response Assessment in Neuro-Oncology Working Group developed new standardized response criteria for clinical trials of brain tumor treatment to evaluate the clinical response to recent treatment including antiangiogenic therapy (40).

REBOUND PHENOMENON AND BEVACIZUMAB CONTINUATION BEYOND PROGRESSION

No effective agent other than TMZ or bevacizumab is available to treat malignant gliomas, and TMZ or bevacizumab therapy, with or without other chemotherapeutic agents, often continues after progressive disease (PD) is observed. Increased doses of TMZ were reported to be beneficial for some patients (41–44). It is unclear whether continued bevacizumab treatment is effective in patients after PD is detected.

Two large observation studies showed that bevacizumab continuation beyond the initial diagnosis of PD improved the OS of patients with metastatic colorectal cancer (45,46). In the BRiTE study, patients with metastatic colorectal cancer receiving first-line bevacizumab with or without chemotherapy received further treatment after the first observation of PD as directed by a physician, and they were observed thereafter. The OS times beyond the first instance of PD for the no post-PD treatment ($n = 253$), post-PD treatment without bevacizumab ($n = 531$) and post-PD treatment with bevacizumab ($n = 642$) groups were 12.6, 19.9 and 31.8 months, respectively. Multivariate analyses demonstrated that the continuation of bevacizumab therapy was strongly and independently associated with improved survival after PD [hazard ratio (HR) = 0.48, $P < 0.001$] (45). Similar results were obtained in the ARIES study (46).

Reardon et al. analyzed the outcomes of patients who received subsequent therapy after PD to evaluate the efficacy of bevacizumab regimens against recurrent GBM in five studies (47). In the studies, bevacizumab was used in combination with irinotecan, daily TMZ, etoposide, bortezomib and erlotinib. The OS times of patients in the no post-PD treatment ($n = 41$), post-PD treatment without bevacizumab ($n = 44$) and post-PD treatment with bevacizumab ($n = 55$) groups were 1.5, 4.0 and 5.9 months, respectively (HR = 0.64, $P = 0.04$). The PFS times of patients in the post-PD treatment without bevacizumab ($n = 44$) and post-PD treatment with bevacizumab ($n = 55$) groups were 1.6 and 2.8 months, respectively (HR = 0.64, $P < 0.0001$). They concluded that bevacizumab continuation beyond the initial detection of PD modestly improves OS compared with available non-bevacizumab therapy for recurrent GBM.

Zuniga et al. (48) reported a rebound phenomenon after the discontinuation of bevacizumab in patients with malignant gliomas. Rebound PD was defined as an increase in the largest cross-sectional area of enhancement on MRI of at least 50% compared with that at the time of bevacizumab failure. Among 40 patients who did not respond to bevacizumab therapy, 11 patients (27.5%) displayed rebound PD, and they had poor prognoses with an OS of 6.8 weeks. Of three patients who were restarted on bevacizumab treatment after rebound PD, two exhibited a partial response, and the OS was extended to 21.3 weeks. Clark et al. (49) analyzed the survival of patients who underwent reoperation and reported that patients who received bevacizumab preoperatively had a worse postoperative OS (HR = 3.1, $P < 0.001$) and PFS than patients who did not receive bevacizumab.

Abrupt discontinuation of bevacizumab after PD may lead to a rebound phenomenon and increased tumor-associated cerebral edema, and therefore, continuation or slow tapering of the bevacizumab dose after PD might be necessary to prevent rebound PD.

NEWLY DIAGNOSED GBM

RT plus TMZ plus bevacizumab was applied for newly diagnosed GBM, and the OS and PFS times were 19.6–23 and 13–13.6 months, respectively (50,51). The efficacy of this combination therapy was superior to that of RT plus TMZ (OS = 14.6 months; PFS = 6.9 months) (1).

A Phase III trial of RT plus TMZ plus placebo vs. RT plus TMZ plus bevacizumab was conducted for 921 patients with newly diagnosed GBMs from 26 countries (52,53). The primary endpoints were PFS and OS, and the final PFS and interim OS results were presented at a Society of Neuro-Oncology meeting at the end of 2012. The PFS times of the placebo ($n = 463$) and bevacizumab groups ($n = 458$) were 4.3 and 8.4 months ($P < 0.0001$, HR = 0.61), respectively, and the addition of bevacizumab to RT plus TMZ significantly extended PFS. The median lengths of time for which patients maintained a Karnofsky performance status